Quantitative Stirling Cycle Measurements: *P-V* Diagram and Refrigeration

Cite as: Phys. Teach. **58**, 18 (2020); https://doi.org/10.1119/1.5141965
Published Online: 23 December 2019

Y. J. Lu, Hiroko Nakahara and J. S. Bobowski

Quantitative Stirling Cycle Measurements: *P-V* Diagram and Refrigeration

Y. J. Lu, Hiroko Nakahara, and J. S. Bobowski, University of British Columbia, Kelowna, BC, Canada

This paper describes simple modifications to a demonstration Stirling engine that allows one to make quantitative measurements of the Stirling cycle. First, we describe measurements of the *P-V* diagram using an inexpensive pressure sensor and a common photogate. Then, as a supplement, the engine was run as a refrigerator by using a rotary tool to turn the flywheel of the engine. A small, but measurable, temperature difference developed across the body of the engine.

Stirling engines have long been used as in-class demonstrations and,[1,2] in some cases, *P-V* diagrams have been constructed using a commercial apparatus.[3,4] It is also worth noting that, despite the fact that Stirling's original patent was filed over 200 year ago, the Stirling cycle is still being actively studied.[5,6] The main objective of our work is to make an accurate measurement of the *P-V* diagram of a high-quality Stirling engine using inexpensive materials and a data acquisition system that is commonly found in undergraduate laboratories.

In an earlier work by Nakahara,[7] the *P-V* diagram was measured using Vernier's Logger Pro data acquisition system. Pressure data were acquired at a rate of 10 samples per second using Vernier's pressure sensor. The gas volume was measured by mounting a reflector onto the piston of the engine and using an infrared (IR) transmitter/receiver to track the piston's position. During operation, the calibrated output voltage of the IR sensor was monitored using Vernier's differential voltage probe.

The advantage of Nakahara's scheme is that it produced a real-time measurement of the *P-V* diagram. There are, however, a number of limitations or disadvantages to this scheme. One is that the pressure sensor does not have the sensitivity to precisely measure the small pressure changes associated with the demonstration Stirling engine. Second, the time between pressure measurements is comparable to the period of the Stirling cycle. Third, the calibration of the IR sensor is nonlinear such that the measurement sensitivity of the piston position is low when the reflector is furthest from the IR transmitter/detector. Finally, to mount the IR sensor, a new top plate for the Stirling engine had to be machined. In this project, we developed a measurement scheme to overcome these limitations, which allowed us to produce high-quality pressure and volume measurements when using the same Stirling engine as Nakahara.

When covering the topic of heat engines in an introductory thermodynamics course, one typically first describes the Carnot cycle.[8] In the Carnot cycle, the isothermal compression of an ideal gas results in heat Q_1 being released to a cold thermal reservoir at temperature T_1, whereas an isothermal expansion causes the gas to absorb heat Q_2 from a hot thermal reservoir at temperature $T_2 > T_1$. The efficiency ε of the cycle is determined by the fraction of the heat removed from the hot reservoir that is converted into useful work W:

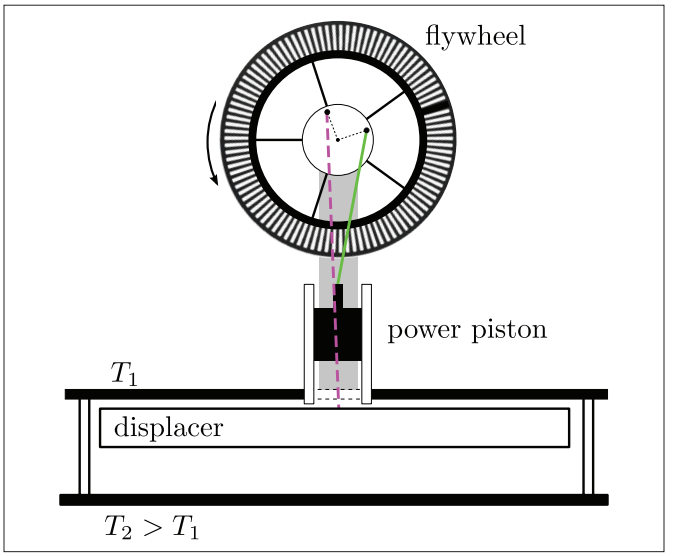

Fig. 1. Schematic diagram of the displacer-style Stirling engine. The power piston and displacer move 90° out of phase with one another. A temperature difference with $T_2 > T_1$ will result in a counterclockwise rotation of the flywheel.

$$\varepsilon = \frac{W}{Q_2} = 1 - \frac{T_1}{T_2}. \quad (1)$$

In addition to the isothermal processes, the Carnot cycle requires an adiabatic compression and expansion to take the gas from T_1 to T_2 and T_2 to T_1, respectively. The Carnot cycle is conceptually simple because there is no heat exchanged between the ideal gas and the thermal reservoirs during the adiabatic processes. The cycle is, however, difficult to implement in practice precisely because one cannot easily isolate the gas from the thermal reservoirs.

The Stirling cycle, on the other hand, is easier to implement but more challenging conceptually since it requires the idea of a regenerator. In the Stirling cycle, the adiabatic processes of the Carnot cycle are replaced with isochoric (constant volume) processes. The isochoric parts of the cycle do no work; however, the gas must absorb (release) heat as its pressure and temperature increases (decreases) at constant volume. This heat exchange occurs via a regenerator through which the gas is forced to pass. The regenerator is typically a porous mesh with a large heat capacity. It can absorb or release a small amount of heat without a substantial change to its temperature. An analysis of the ideal Stirling cycle shows that it has the same efficiency, given by Eq. (1), as the Carnot cycle.

The Stirling cycle is more practical because the constant volume processes can be implemented in a number of different ways. The Stirling engine used in our project is made by Kontax Stirling Engines.[9] The main elements of the engine,

 DOI: 10.1119/1.5141965

shown schematically in Fig. 1, are a power piston that sets the volume of the working gas, a displacer that is used to move the gas between the hot and cold regions of the engine, and a flywheel. The positions of the piston and displacer are set by connecting rods that are attached to a disk centered on the flywheel. As shown in the figure, the connecting rods are attached such that the piston and displacer positions and speeds are 90° out of phase with one another. In Fig. 1, an (approximately) isothermal expansion of the gas while it is in contact with the hot reservoir results in a counterclockwise rotation of the flywheel. This would be followed by an (approximately) isochoric process that would decrease the gas temperature from T_2 to T_1.

This displacer-style Stirling engine does not have a porous regenerator through which the gas passes during the constant volume processes. However, the surface of the displacer and the cylindrical wall separating the hot and cold thermal reservoirs together act as a crude regenerator. With such a poor regenerator, the work output per cycle will be low and the engine's efficiency is expected to be much less than that of the ideal Stirling cycle.

P-V diagram

Figure 2 shows the experimental setup used to simultaneously measure the pressure and volume of the displacer-type Stirling engine.

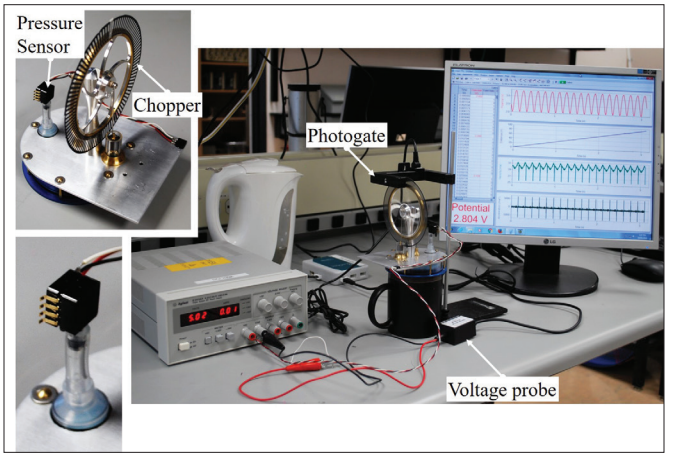

Fig. 2. Photograph of the setup to measure the Stirling cycle *P-V* diagram. A photogate and chopper are used to sense the position of the power piston while a pressure sensor and voltage probe monitor the gas pressure.

Pressure measurement —

To monitor the pressure change of the gas in the Stirling engine, an inexpensive differential pressure sensor was purchased. From Nakahara's previous work, the pressure change was expected to be just over 1 kPa. Therefore, we purchased the MPXV7002 pressure sensor manufactured by NXP Semiconductors, which has a voltage output that varies from 0.5 to 4.5 V for pressure changes from -2 to +2 kPa.[10]

To connect the pressure sensor to the Stirling engine, a hole was drilled through the engine's aluminum top plate to accommodate the tip of a Luer lock syringe. The syringe was epoxied in place using J-B Weld. As shown in Fig. 2, the pressure sensor was then connected to the syringe tip using tight-fitting rubber tubing. During operation, the pressure sensor's output voltage was recorded at a rate of 200 samples/s using Vernier's Logger Pro software and differential voltage probe.

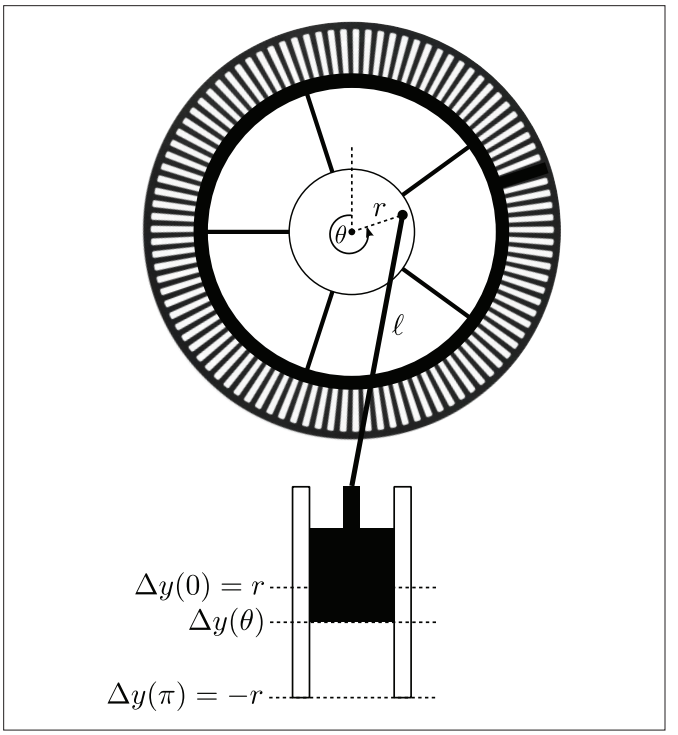

Fig. 3. The geometry used to convert flywheel position in radians to piston height Δ*y*.

Volume measurement –

To calculate the change in gas volume, the height of the Stirling engine's piston was measured. A circular chopper with $N_0 = 100$ intervals and a photogate were used to track the rotation of the engine's flywheel. As illustrated in Fig. 3, the chopper was attached to the flywheel and oriented such that a single intentionally blackened interval was at the top ($\theta = 0$) when the piston was at its maximum height.

Figure 3 also shows the geometry that relates the flywheel rotation to the piston height. A careful analysis of this geometry reveals that the change in piston height is given by

$$\Delta y = r\left[\cos\theta - \frac{\ell}{r}\left(\sqrt{1-\left(\frac{r}{\ell}\sin\theta\right)^2} - 1\right)\right] \tag{2}$$

$$\approx r\left[\cos\theta + \frac{r}{2\ell}\sin^2\theta\right], \tag{3}$$

where the approximate expression is valid when $r \ll \ell$. The change in volume is then given by Δy times the cross-sectional area of the piston.

The angular position of the flywheel was monitored using a Vernier photogate and Logger Pro. The software was set to record the times at which the photogate went from a blocked to an unblocked state. Under these conditions, after passing through the $\theta = 0$ point, the first angle recorded, in units of radians, is $(3/4)(2\pi/N_0)$. The factor of 3/4 is due to the fact that $\theta = 0$ corresponds to the midpoint of the chopper section that has been intentionally blocked. The subsequent θ measure-

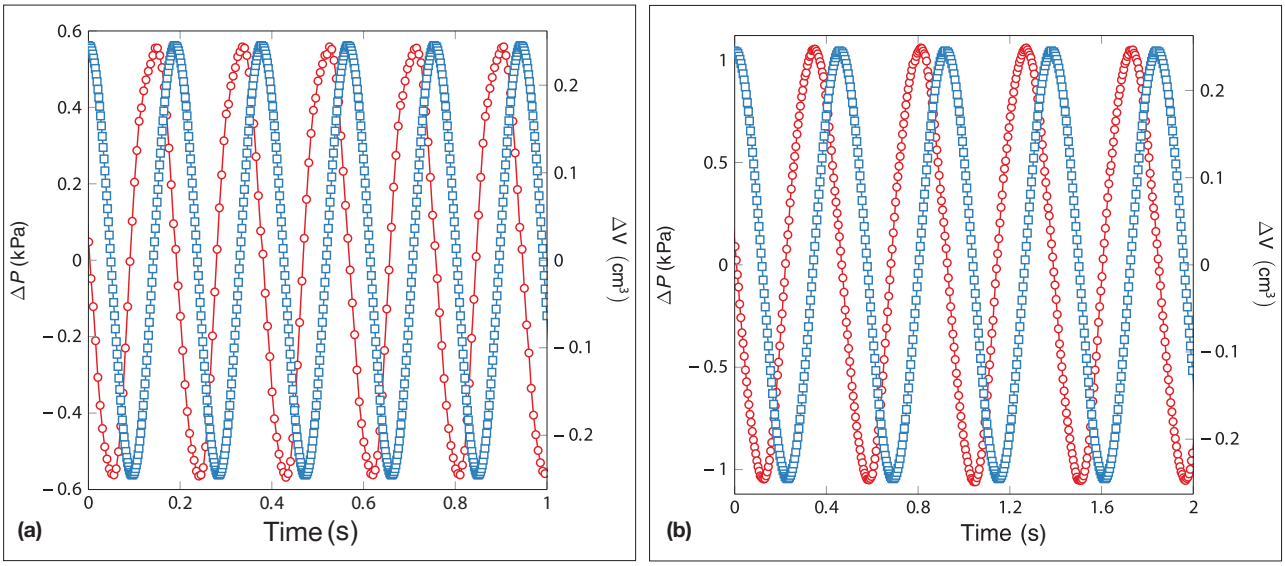

Fig. 4. (a) Measured change in pressure (red circles) and volume (blue squares) vs. time with a free-running flywheel. (b) Measured change in pressure (red circles) and volume (blue squares) vs. time with light friction applied to the flywheel.

ments increment in steps of $2\pi/N_0$. In general, the angle at the n^{th} recorded time is given by

$$\theta_n = \frac{2\pi}{N_0}\left(n - \frac{1}{4}\right), \tag{4}$$

where n is an integer that runs from 1 to $N_0 - 1$.

Results

Figure 4(a) shows the measured pressure and volume changes of the Kontax Stirling engine as a function of time. For these data, the Stirling engine was placed on top of a cup of hot water. The data acquisition was started after the Stirling engine reached a steady speed. The data are high resolution and the acquisition rate is high compared to the speed of the engine ($\approx$ 5.3 cycles/s). The data also convincingly show that the pressure and volume changes are 90° out of phase and that the pressure leads the volume.

In Fig. 5, we show a plot of the Stirling engine's *P-V* diagram. The *P-V* diagram that corresponds to the data in Fig. 4(a) is shown using orange circles. Because Logger Pro records the pressure and photogate readings at different times, an interpolation function was used to determine the volume changes at the times of the pressure readings. The plot in Fig. 5 shows a set of 25 consecutive cycles that are indistinguishable from one another.

Clearly, the measured *P-V* diagram differs from that of the ideal Stirling cycle. For truly isothermal processes, and when ΔV is small compared to the absolute volume, as is the case here, one expects $\Delta P \propto -\Delta V$. The differences between our measured cycle and the ideal Stirling cycle could, in part, be due to the absence of a true regenerator in the displacer-style Stirling engine used in our experiments. Also, as expected from the design of the connecting rods, there are no perfectly isochoric processes in our measured cycle.

The high-resolution data do, nevertheless, allow for an accurate measurement of the area enclosed by the loop which gives the work output by the engine per cycle. The work done

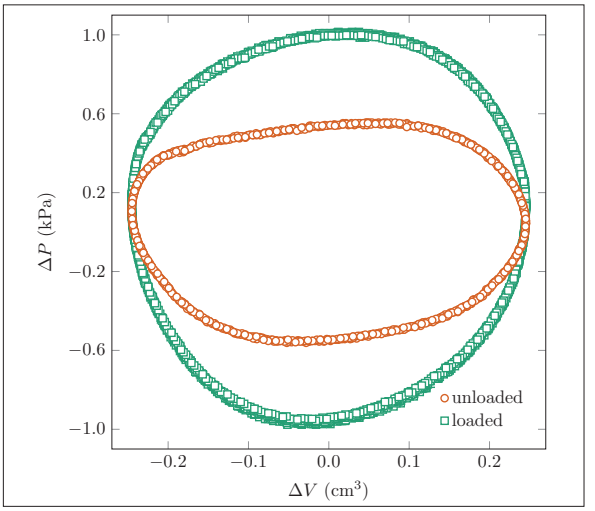

Fig. 5. Measured *P-V* diagram of the Kontax Stirling engine with (green squares) and without (orange circles) friction applied to the flywheel. The added friction causes the engine to do more work per cycle while simultaneously reducing the power output.

from measurement i to $i + 1$ is given by

$$W_i = \left(\frac{\Delta P_{i+1} + \Delta P_i}{2}\right)(\Delta V_{i+1} - \Delta V_i). \tag{5}$$

Summing all of the W_i contributions from one complete cycle gives the net work, which was found to be 0.43 mJ. The enclosed area can also be estimated by approximating the loop as an ellipse that has an area given by πab, where a and b are the lengths of the semi-major and semi-minor axes, respectively. Multiplying the net work by the cycle rate of 5.3 Hz gives an output power of 2.3 mW, or 3.0 micro-horsepower!

Finally, the measurements of ΔP and ΔV were repeated after light friction was applied to the flywheel of the Stirling engine. A small piece of sponge was attached to a retort stand and then brought into light contact with the flywheel while the engine was running. The pressure and volume changes are

plotted as a function of time in Fig. 4(b). These data show the same 90° phase shift between the pressure and volume. Notice, however, that the magnitude of the pressure change approximately doubled and the period of the cycle increased from 0.19 s for the free-running engine to 0.43 s after applying friction.

The *P-V* diagram that corresponds to the data in Fig. 4(b) is shown using green squares in Fig. 5. Again, 25 consecutive and nearly identical cycles are shown. The increase in enclosed area is an indication that the engine is doing more work per cycle (0.75 mJ) when friction is applied to the flywheel. However, the power output, obtained by dividing the work per cycle by the period, was 1.7 mW, which is 20% below that of the free-running engine.[5]

Refrigeration

Today, the most common commercial application of the Stirling cycle is in closed-cycle cryocoolers.[11] In a cryocooler, mechanical work is done on the working gas to generate a temperature difference. Several companies now make single-stage Stirling cryocoolers capable of reaching 40 K and two-stage systems capable of reaching lower temperatures. For a review of modern cryocooler technology, see Ref. 12.

To run the Kontax Stirling engine as a cryocooler, it was first necessary to thermally isolate the top and bottom plates of the engine from the surrounding environment. A 2-in sheet of high-density polystyrene foam was cut using a hot 32-AWG nichrome wire. The wire was under tension and we found that a current of 1 A was sufficient to make clean cuts. As shown

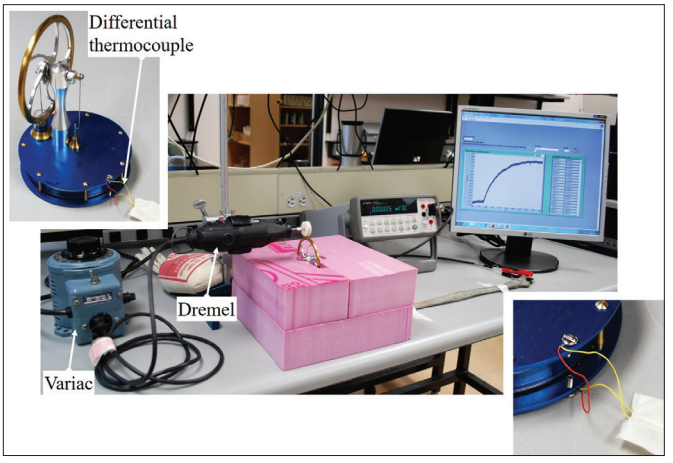

Fig. 6. Photograph of the setup used to operate the Kontax Stirling engine as a refrigerator. A Dremel tool was used to rotate the flywheel and a differential thermocouple measured the temperature difference between the top and bottom plates of the engine.

in Fig. 6, polystyrene blocks were cut such that the Stirling engine was completely enclosed except for the upper half of the flywheel.

The lower-right corner of Fig. 6 shows the differential thermocouple that was used to monitor the temperature difference between the top and bottom plates of the Stirling engine. A single #4-40 tapped hole was drilled into each of the top and bottom plates, and screws were used to clamp down on the junctions of a type-E thermocouple. Fine thermocouple wires were used so as to limit heat conduction along the wires as much as possible. The thermocouple voltage was measured using a Keysight 34401A multimeter. The data were logged as a function of time using a simple LabVIEW program.

The flywheel of the Stirling engine was rotated using a Dremel tool and a polishing felt attachment. Even when on its lowest setting, the Dremel spins the flywheel too fast to produce reliable results. We found that when the flywheel was rotated too fast, the dominant effect was heating of the top plate by friction. The best results were obtained when the flywheel was rotated at a rate between 1 and 2 Hz. To reduce the speed of the Dremel, it was plugged into a variac that was set to approximately 25 Vrms.

Figure 7 shows the difference in temperature between the top and bottom plates of the Stirling engine as a function to time. The raw data are shown by the gray data points. Initially, the Dremel was off and the flywheel was stationary. The Dremel was started at approximately 50 min and allowed to run continuously for 30 min. During that time, the temperature difference increased and was beginning to plateau by the end of the 30 min runtime. An increasing ΔT corresponds to the top plate warming relative to the bottom plate. After the Dremel was stopped, the temperature difference steadily decreased. The Dremel was run for another 30-min interval starting at approximately 110 min. However, for this run the rotation direction of the flywheel was reversed. As expected, this caused the top plate to cool relative to the bottom plate. The Dremel was stopped at 140 min.

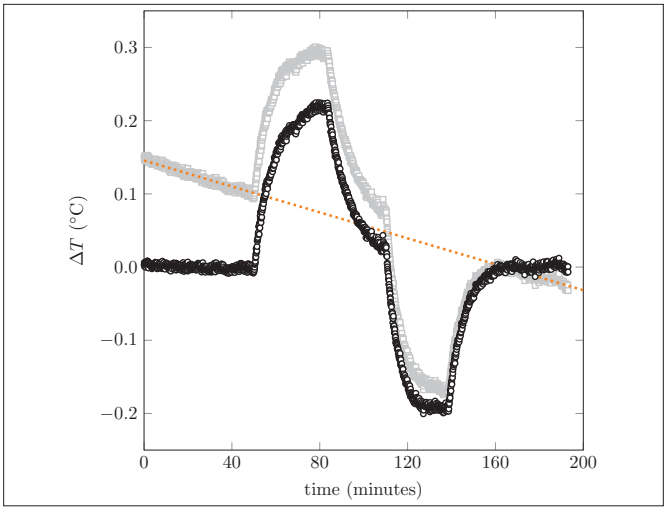

Fig. 7. Measured temperature difference across the top and bottom plates of the Stirling engine vs. time. The raw ΔT data are shown by grey data points. The black data points show ΔT after removing the background drift of the room temperature, shown by the dotted line. A positive ΔT indicates that the top plate is at a higher temperature than the bottom plate.

Figure 7 clearly shows a nonzero ΔT that evolves linearly with time even when the Dremel has been stopped for an extended period of time. This is due to a slow drift of the room temperature. The polystyrene used to isolate the Stirling engine from its surroundings has a hole in the top to accommodate the flywheel. Therefore, the top plate of the engine

is more sensitive to changes in room temperature than the bottom plate, which results in the observed drift in ΔT. The gray data from 0 to 48 min and from 160 to 190 min were fit to a straight line. The best fit line has a slope of -0.89×10^{-3} °C/min and is shown in Fig. 7 as the dotted orange line. The black data in the figure show ΔT after removing the drift caused by the changing room temperature. The result is an approximately symmetric ΔT that reaches ± 0.2 °C after running the Dremel for about 30 min.

Summary

Stirling engines are commonly used as a demonstration of a working heat engine. These demonstrations can be significantly enhanced by adding instrumentation to measure the pressure and volume changes of a running engine. We have described a simple and inexpensive way to instrument a high-quality Stirling engine designed for demonstrations. Our pressure vs. time measurements are high resolution and reveal the 90° phase shift between the pressure and volume changes. The *P-V* diagram constructed from these measurements allows one to determine the net work by the engine per cycle and, therefore, the power output. By adding friction to the flywheel, it was shown that the work per cycle increased while the power output decreased. Finally, we used a rotary tool to drive the flywheel of the Stirling engine while monitoring the temperature difference across its body. A small, but measurable, temperature difference was observed. Reversing the flywheel rotation direction reversed the sign of the observed temperature difference.

References

1. R. D. Spence and C. L. Foiles, "Stirling engines for demonstration," *Phys. Teach.* **20**, 38 (Jan. 1982).
2. H. R. Crane, "The Stirling engine—173 years old and running," *Phys. Teach.* **28**, 252 (April 1990).
3. C. G. Deacon, R. Goulding, C. Haridass, and B. de Young, "Demonstration experiments with a Stirling engine," *Phys. Educ.* **29**, 180 (May 1994).
4. M. D. Kutzner and M. Plantak, "Complete cycle experiments using the adiabatic gas law apparatus," *Phys. Teach.* **52**, 418 (Oct. 2014).
5. R. A. Simon, "Stirling's cycle and the second law of thermodynamics," *Am. J. Phys.* **52**, 496 (June 1984).
6. A. Romanelli, "Alternative thermodynamic cycle for the Stirling machine," *Am. J. Phys.* **85**, 926 (Dec. 2017).
7. H. Nakahara, "Displacer-type Stirling engine," https://people. ok.ubc.ca/jbobowsk/Stirling/introduction.html.
8. D. V. Schroeder, *An Introduction to Thermal Physics* (Pearson Education, Inc., San Francisco, 1999), pp. 122–136.
9. We purchased the KS90 Blue Stirling engine from Kontax Stirling engines. These engines can be purchased online from the company website, https://www.stirlingengine.co.uk.
10. MPXV7002 Integrated Silicon Pressure Sensor On-Chip Signal Conditioned, Temperature Compensated and Calibrated, Rev. 4 ed., NXP Semiconductors, https://www.nxp.com.
11. J. W. L. Köhler, "The Stirling refrigeration cycle," *Sci. Am.* **212**, 119 (April 1965).
12. R. Radebaugh, "Cryocoolers: The state of the art and recent developments," *J. Phys. Condens. Matter* **21**, 164219 (April 2009).

University of British Columbia, Kelowna, BC, Canada
Jake.Bobowski@ubc.ca